DY Pegasi: An SX Phoenicis Star in a Binary System with an Evolved Companion

Hui-Fang Xue[1] and Jia-Shu Niu[2, 3, 4]

[1] Department of Physics, Taiyuan Normal University, Jinzhong, 030619, China
[2] Institute of Theoretical Physics, Shanxi University, Taiyuan 030006, China
[3] State Key Laboratory of Quantum Optics and Quantum Optics Devices, Shanxi University, Taiyuan 030006, China
[4] Collaborative Innovation Center of Extreme Optics, Shanxi University, Taiyuan, Shanxi 030006, China

ABSTRACT

In this work, the photometric data from the American Association of Variable Star Observers are collected and analyzed on the SX Phoenicis star DY Pegasi (DY Peg). From the frequency analysis, we get three independent frequencies: $f_0 = 13.71249$ c days^{-1}, $f_1 = 17.7000$ c days^{-1}, and $f_2 = 18.138$ c days^{-1}, in which f_0 and f_1 are the radial fundamental and first overtone mode, respectively, while f_2 is detected for the first time and should belong to a nonradial mode. The $O - C$ diagram of the times of maximum light shows that DY Peg has a period change rate $(1/P_0)(dP_0/dt) = -(5.87 \pm 0.03) \times 10^{-8}$ yr^{-1} for its fundamental pulsation mode, and should belong to a binary system that has an orbital period $P_{\rm orb} = 15425.0 \pm 205.7$ days. Based on the spectroscopic information, single star evolutionary models are constructed to fit the observed frequencies. However, some important parameters of the fitted models are not consistent with that from observations. Combing with the information from observation and theoretical calculation, we conclude that DY Peg should be an SX Phoenicis star in a binary system and accreting mass from a dust disk, which was the residue of its evolved companion (most probably a hot white dwarf at the present stage) produced in the asymptotic giant branch phase. Further observations are needed to confirm this inference, and it might be potentially a universal formation mechanism and evolutionary history for SX Phoenicis stars.

1. INTRODUCTION

SX Phoenicis (SX Phe) stars, a subgroup of the high-amplitude δ Scuti stars (HADS), are old Population II stars. They always pulsate in single or double radial modes (such as SW Ser, AE UMa, etc.), but some also show nonradial modes coupling with the radial modes. Because of the insufficient amount and the generally poor photometric precision of the observation data, whether any low-amplitude pulsations exist besides the dominant radial modes in most SX Phe stars is still unknown. Although most SX Phe stars, which are characterized by high amplitudes of pulsation, low metallicity, and large spatial motion, are found to be members of globular clusters (Rodríguez & López-González 2000), some of them have been discovered in the general star fields (Rodríguez & Breger 2001). In particular, pulsations in the majority of the field SX Phe variables display very simple frequency spectra with short periods ($\leq 0^{\rm d}.08$) and large visual peak-to-peak ampli-

tudes ($\geq 0^{\rm m}.1$; see Fu et al. (2008)). There are several scenarios proposed to illustrate the formation mechanism and evolutionary history of SX Phe stars (see, e.g., Rodríguez & López-González (2000)), but the origin of them is still unknown up to now.

DY Peg is an SX Phe star with a low metallicity ([Fe/H] $= -0.8$, Burki & Meylan (1986) and Hintz et al. (2004); [Fe/H] $= -0.56$, Peña et al. (1999)). The variability of DY Peg was discovered by Morgenroth (1934), whereafter a good amount of photometric monitoring was done to record and analyze its behavior of lightness variation (see, e.g., Iriarte (1952); Meylan et al. (1986); Percy et al. (2007)). Based on the secular observations, the period change of DY Peg was continuously studied in history (see, e.g., Quigley & Africano (1979); Mahdy & Szeidl (1980); Pena & Peniche (1986); Derekas et al. (2003); Hintz et al. (2004); Derekas et al. (2009); Fu et al. (2009)). Li & Qian (2010) did a more detailed research on the period change of this star, in which they reported the variation of the period can be described by a secular decrease of the period at a rate of -6.59×10^{-13} days cycle^{-1}, and a perturbation from a companion star in an eccentric orbit with a period of 15414.5 days. Unlike the period change that has

Corresponding author: Jia-Shu Niu
jsniu@sxu.edu.cn

been studied adequately, the pulsation frequency of DY Peg was not detected accurately beside the fundamental mode. Garrido & Rodriguez (1996) and Pop et al. (2003) reported that DY Peg should be a double-mode pulsator, while it was not confirmed in subsequent works (Fu et al. 2009; Barcza & Benkő 2014).

In the following sections, we extract some important information from observations, construct theoretical models and present some discrepancies between observation and theoretical calculation. Then, we propose some inferences to relieve the discrepancies and backtrack the evolutionary history of DY Peg. This paper is organized as follows: Section 2 presents the data reduction procedures from observations; theoretical models are constructed and the calculation results are shown in Section 3; Section 4 gives the discussion and conclusions.

2. OBSERVATIONS AND ANALYSIS

2.1. *Observations*

The time-series photometric data in the V band on DY Peg is downloaded from the American Association of Variable Star Observers (AAVSO) International Database (Kafka 2020), which cover from 2003 August to 2019 December. After the heliocentric corrections of the Julian date and magnitude shifts elimination between different nights, the light curves are used to extract the times of maximum light (see Figure 1). A portion of the light curves covering a period of 32 days (from 2011 October 30 to 2011 December 1) are used to make frequency analysis. Table 1 lists the detailed information of the observations for the frequency analysis, and Figure 2 shows the relevant light curves.

2.2. *Frequency Analysis*

The software Period04 (Lenz & Breger 2005) is used to perform Fourier transformations and frequency pre-whitening process for the light curves of DY Peg. Figure 3 shows the spectral window and Fourier amplitude spectra of the pre-whitening process. The statistical criterion of an amplitude signal-to-noise ratio is set to be 4.0 for judging the reality of a newly discovered peak in the Fourier spectra. The noises are determined as the mean amplitudes around each peak with a box of 6 c days^{-1}.

In total, 14 statistically significant frequencies have been detected, including 3 independent frequencies ($f_0 = 13.71249$ c days^{-1}, $f_1 = 17.7000$ c days^{-1}, and $f_2 = 18.138$ c days^{-1}), together with 11 harmonics or linear combinations of them. The solid curves in Figure 2 show the fits with the multi-frequency solution which is listed in Table 2.

The first pulsation mode with frequency $f_0 = 13.71249$ c days^{-1} and amplitude $a_0 = 240.3$ mmag dominates the light curves of DY Peg. The secondary pulsation mode with frequency $f_1 = 17.7000$ c days^{-1} and a small amplitude $a_1 = 5.2$ mmag is obvious in the present work, which was not confirmed in previous works because of the low signal-to-noise (see Garrido & Rodriguez (1996), Pop et al. (2003), Fu et al. (2009), and Barcza & Benkő (2014)).

The ratio of $f_0/f_1 = 0.775$ agrees well with the theoretical calculation on the fundamental and first overtone radial modes (~ 0.77, see Petersen & Christensen-Dalsgaard (1996); Poretti et al. (2005)), illustrating DY Peg does pulsate in the two radial modes.

What is interesting is that a third independent frequency solution with frequency $f_2 = 18.138$ c days^{-1} and amplitude $a_2 = 2.8$ mmag is detected in this work, for the first time. The frequency f_2 is close to f_1 with a smaller amplitude, therefore, we suggest that f_2 should be a nonradial mode.[1] For a definite mode identification of f_2, multicolour photometry or time resolved high resolution spectroscopy is needed.

2.3. *The $O-C$ Diagram* [2]

Based on the observations between 2003 and 2019 (see Figure 1), the light curves around the maxima were fitted by a fourth polynomial. We have obtained 139 times of maximum light from these light curves, and estimated their uncertainties via Monte Carlo simulations. The newly determined times of maximum light and the uncertainties are listed in Table C1. In Li & Qian (2010), 412 times of light maximum of DY Peg obtained from photoelectric or CCD data had been collected, which are also used in our $O-C$ analysis. In addition, 138 times of maximum light in the V band are collected from the literature, which are listed in Table C2. In total, 689 times of maximum light spanning 70 years are used to perform the $O-C$ analysis in this work. [3]

As it has been shown by Li & Qian (2010), a linear or quadratic fit cannot reproduce the times of light maximum precisely. Consequently, we fit the times of light maximum with a quadratic plus a function of sines,

---

[1] The ratio of $f_0/f_2 = 0.756$ can rule out the assumption that f_2 is a radial mode.

[2] Because the amplitude of f_0 is about 46 times larger than that of f_1 and the times of maximum light are dominated by the f_0 mode, $O-C$ method can be used effectively to analyze the pulsating and orbital parameters in this case.

[3] In the following analysis, we give typical uncertainties of 0.0006 days and 0.0005 days to the times of maximum light in the literature detected by photoelectric photometers and CCD cameras, respectively, which did not give corresponding uncertainties.
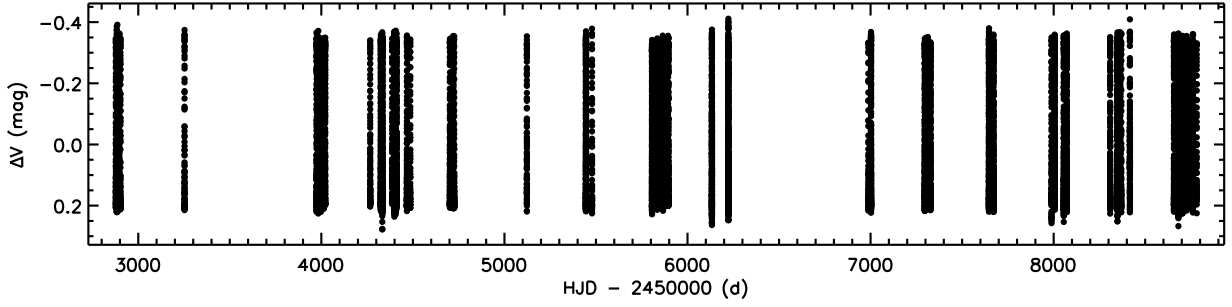
Figure 1. Light curves of DY Peg from 2003 August to 2019 December.

Table 1. Detailed information of the observations for frequency analysis.

Date	Duration (hours)	Number of Observations	σ (mag)
2011 Oct 30	6.7	144	0.001
2011 Nov 1	6.0	127	0.001
2011 Nov 2	6.7	142	0.001
2011 Nov 4	4.2	88	0.001
2011 Nov 11	4.7	100	0.001
2011 Nov 18	5.6	120	0.001
2011 Nov 28	5.0	103	0.001
2011 Nov 29	4.8	94	0.001
2011 Dec 1	4.8	99	0.001

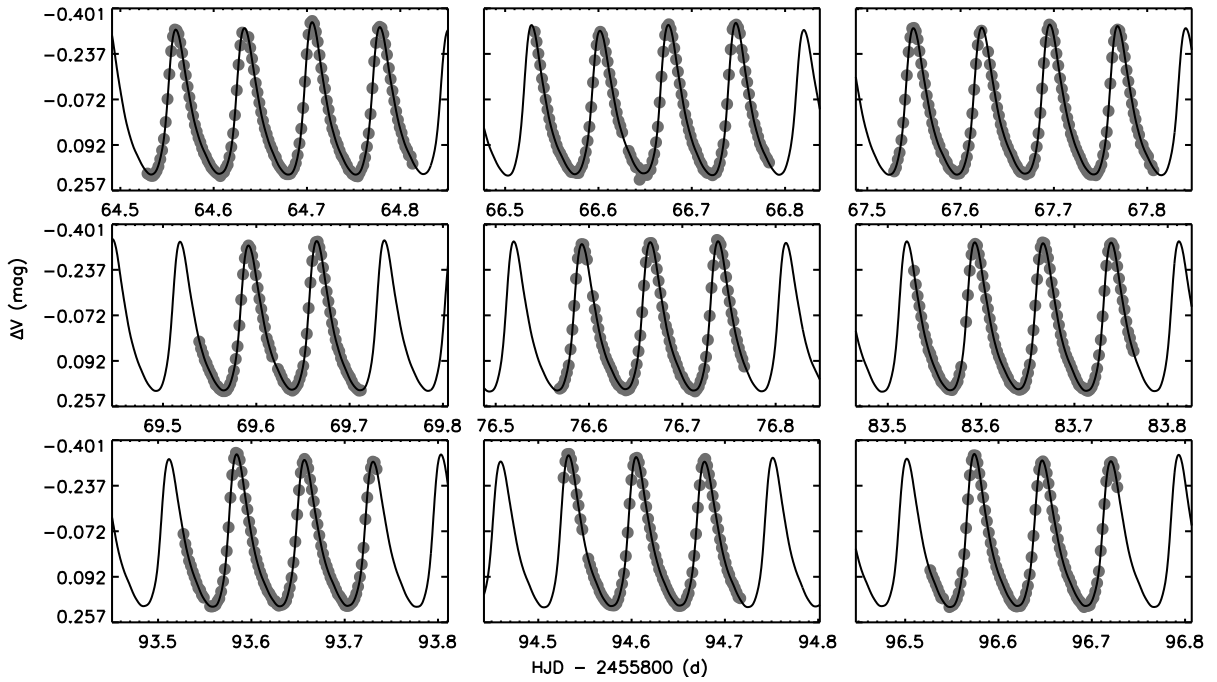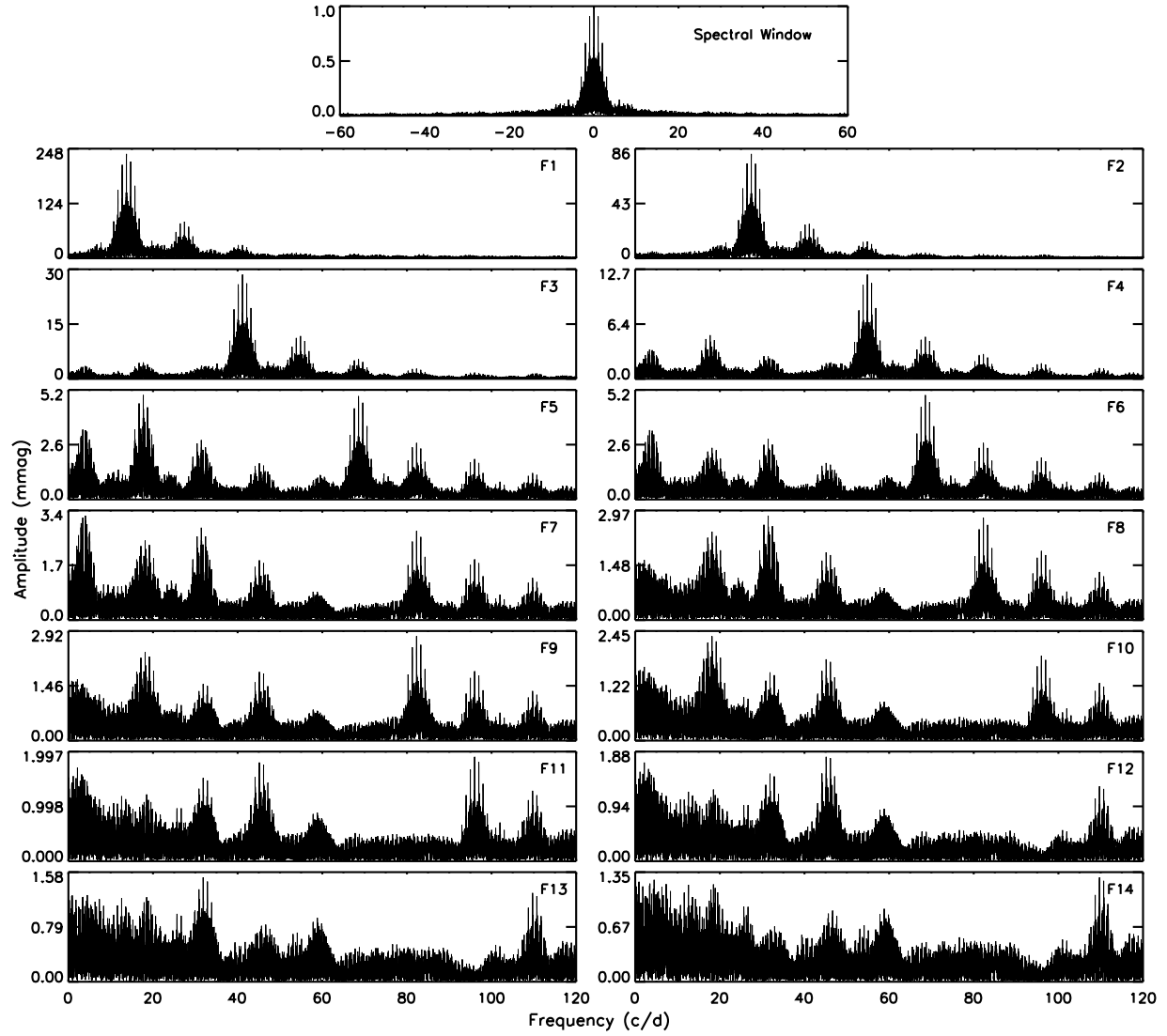NOTE—σ denotes the mean error of the observations.

Figure 2. Light curves of DY Peg covering a period of 32 days since 2011 October 30. The solid curves show the fits with the multifrequency solution.

Figure 3. Spectral window and Fourier amplitude spectra of the frequency pre-whitenning process for the light curves of DY Peg.

Table 2. Multi-frequency solution of the light curves of DY Peg in 2011.

NO.	Marks	Frequency (c days^{-1})	σ_f (c days^{-1})	Amplitude (mmag)	σ_a (mmag)	S/N
F1	f_0	13.71249	0.00001	240.3	0.2	112.6
F2	$2f_0$	27.42506	0.00004	82.2	0.2	104.2
F3	$3f_0$	41.1374	0.0001	28.3	0.2	68.8
F4	$4f_0$	54.8502	0.0003	12.1	0.2	45.2
F5	f_1	17.7000	0.0006	5.2	0.2	6.6
F6	$5f_0$	68.5626	0.0007	5.0	0.2	25.7
F7	$f_1 - f_0$	4.016	0.001	2.9	0.2	4.8
F8	$f_0 + f_1$	31.412	0.001	2.7	0.2	6.1
F9	$6f_0$	82.275	0.001	2.7	0.2	13.4
F10	f_2	18.138	0.001	2.8	0.2	6.7
F11	$7f_0$	95.987	0.002	1.8	0.2	16.4
F12	$2f_0 + f_1$	45.122	0.002	1.7	0.2	6.1
F13	$f_0 + f_2$	31.851	0.002	1.7	0.2	6.8
F14	$8f_0$	109.702	0.003	1.2	0.2	6.7

NOTE—σ_f denotes the error estimation of frequency, σ_a denotes the error estimation of amplitude. All of them are calculated based on the formulas given by Montgomery & Odonoghue (1999).

which imply they are affected by the linear change of the pulsation period of the star and by a light traveling time effect of the star in a binary system of an elliptical orbit (Paparo et al. 1988). The calculated times of light maximum have the form

$$C = \text{HJD}_0 + P_0 \times E + \frac{1}{2}\beta E^2 + \\ A[\sqrt{1 - e^2}\sin\phi\cos\omega + \cos\phi\sin\omega], \tag{1}$$

where ϕ is the solution of Kepler's equation

$$\phi - e\sin\phi = \frac{2\pi}{P_{\text{orb}}}(P_0 \times E - t_0). \tag{2}$$

In the above formulas, HJD_0 is the initial epoch, P_0 is the pulsation period, β is the linear change of pulsation period, $A = a_1 \sin i/c$ (c is the speed of light in vacuum) is the projected semi-major axis, e is the eccentricity, ϕ is the eccentric anomaly, ω (the argument of periastron) is the angle from the ascending node to periastron in the orbital plane, P_{orb} is the orbital period of the binary **system**, and t_0 is the time of passage through the periastron. We present a brief mathematical deduction of the above equations in Section B of the Appendix. More details of the light-time orbit equation can be found in Irwin (1952).

The Markov Chain Monte Carlo (MCMC) algorithm is used to determine the posterior probability distribu-

tion of the parameters in Eq. (1) and (2).[4] The samples of the parameters are taken as their posterior probability distribution function (PDF) after the Markov Chains have reached their equilibrium states. The mean values and the standard deviation of the parameters are listed in Table 3, and the best-fit result (which gives $\chi^2/\text{d.o.f.} = 61.57$) of the $O - C$ values (excluding the linear part) and the corresponding residuals are shown in Figure 4.

Benefiting from the extension of nearly 10 years of times of maximum light, the solution of orbital parameters are obviously refined compared with that in Li & Qian (2010). The uncertainties of β, A, and e are about one tenth of that in Li & Qian (2010). Moreover, some parameters are seriously corrected in this work: β, A, and ω have corrections of about 30%, while e has a correction of about 60%. All these refinements provide us highly credible results for the subsequent discussion.

3. THEORETICAL MODELS

Considering the orbital period $P_{\text{orb}} \sim 15400$ days, which is so large that DY Peg could not have an evolutionary history with severe mass transfer like that in the case of planetary nebulae (PNe) with binary central stars (see, e.g., Jones & Boffin (2017)), we attempt to determine its stellar mass and evolutionary stage based

---

[4] The PYTHON module emcee (Foreman-Mackey et al. 2013) is employed to perform the MCMC sampling. Some examples can be found in Niu & Li (2018); Niu et al. (2018, 2019) and references therein.
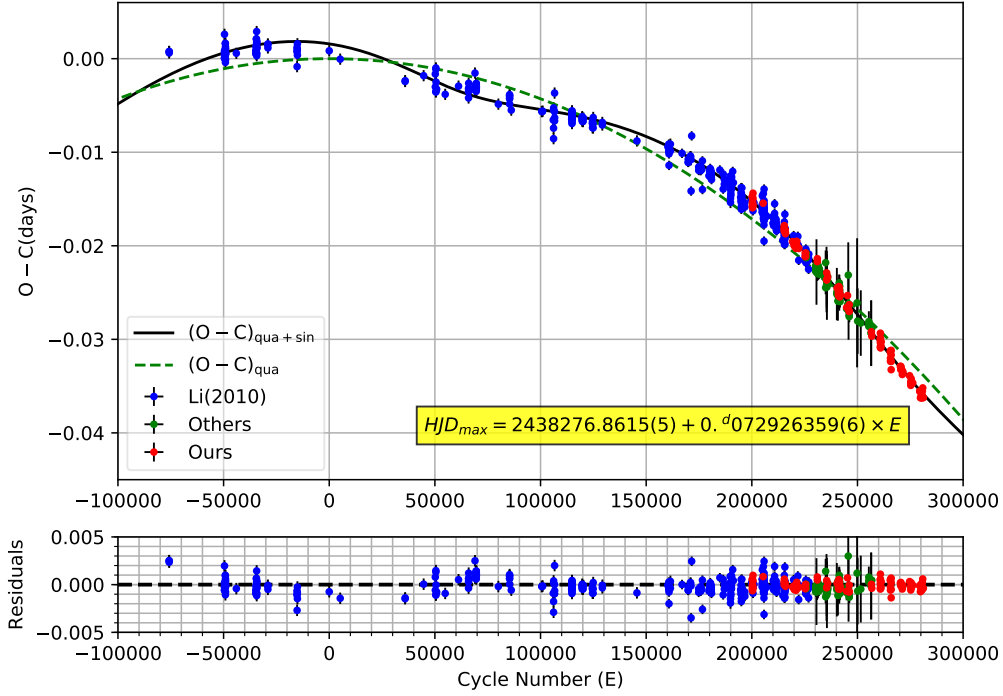
Figure 4. $O - C$ values (excluding the linear part $\mathrm{HJD_{max}}$) and the corresponding residuals. In the upper panel, the black line represents the best-fit result of a quadratic plus a light-time orbit equation, and the green dashed line represents the quadratic part. In the lower panel, the residuals of the best-fit result are plotted. The data collected from Li & Qian (2010) are shown in blue points; the data from historical literature are shown in green points; the data from present work are shown in red points.

Table 3. The pulsating and orbital parameters of DY Peg from this work and Li & Qian (2010).

Parameter	Value of this work	Value of Li & Qian (2010)
$\mathrm{HJD_0}$	$2438276.86155 \pm 0.00007$	$2438276.86149 \pm 0.00013$
P_0 (days)	$0.0729263596 \pm 0.0000000006$	$0.0729263444 \pm 0.0000000028$
β (day cycle^{-1})	$(-8.55 \pm 0.04) \times 10^{-13}$	$(-6.59 \pm 0.38) \times 10^{-13}$
A (days)	0.00204 ± 0.00003	0.00147 ± 0.00020
e	0.244 ± 0.008	0.65 ± 0.10
P_{orb} (days)	15425.0 ± 205.7	15414.5 ± 548.8
t_0	2457941.8 ± 158.7	2454074.1 ± 233.3
ω	239.3 ± 5.2	180.7 ± 10.3
$a_1 \sin i$ (AU)	0.353 ± 0.005	0.254 ± 0.034
$(1/P_0)(\,\mathrm{d}P_0/\,\mathrm{d}t)$ (yr^{-1})	$-(5.87 \pm 0.03) \times 10^{-8}$	—
$f(M)$ (M$_\odot$)	$(2.47 \pm 0.12) \times 10^{-5}$	—

NOTE—the values of $a_1 \sin i$ and $(1/P_0)(\,\mathrm{d}P_0/\,\mathrm{d}t)$ are derived from the values of A and β respectively. The value of $f(M)$ (mass function) is derived from the values of $a_1 \sin i$ and P_{orb}.

on the single star evolutionary models (see, e.g., Niu et al. (2017); Xue et al. (2018)).

The open source 1D stellar evolution code Modules for Experiments in Stellar Astrophysics (MESA, Paxton et al. (2011, 2013, 2015, 2018, 2019), and references therein) is used to construct the structure and evolutionary models. The stellar oscillation code GYRE (Townsend & Teitler 2013) is used to compute the corresponding pulsation frequencies for a specific structure model.

The initial parameters that are used to construct pre-main sequence evolutionary models of DY Peg are configured as follows. Different metallicity [Fe/H] with the values of -1.0, -0.8, and -0.56 dex are considered as the initial metallicity of the evolutionary model (see Table 4 for more details). The following formulas are used to calculate the initial heavy element abundance Z and initial hydrogen abundance X:

$$[\text{Fe/H}] = \log \frac{Z}{X} - \log \frac{Z_\odot}{X_\odot}, \qquad (3)$$

$$Y = 0.24 + 3Z, \qquad (4)$$

$$X + Y + Z = 1, \qquad (5)$$

where $X_\odot = 0.7381$ and $Z_\odot = 0.0134$ (Asplund et al. 2009). Equation (4) is provided by Mowlavi et al. (1998). Based on the given values of [Fe/H], we get $(X = 0.756, Z = 0.001)$, $(X = 0.752, Z = 0.002)$, and $(X = 0.744, Z = 0.004)$ as the initial inputs of the evolutionary models. The initial mass of the models is set in the interval from 0.8 M$_\odot$ to 2.0 M$_\odot$ with a step of 0.01 M$_\odot$, covering the typical mass range of SX Phe stars (McNamara 2011). In the model calculation, the rotation of the star has also been considered. Because Solano & Fernley (1997) provides us with the projected rotational velocity $v \sin i = 23.6$ km s^{-1}, the equatorial rotation velocities $v_{\text{eq}} = 23.6$ km s^{-1} and $v_{\text{eq}} = 150$ km s^{-1} are set to be the inputs in the model calculation, which covers a reasonable range of $\sin i$. The value of the mixing-length parameter is set to be $\alpha_{\text{MLT}} = 1.89$ (see Yang et al. (2012)). Every evolutionary track is calculated from zero-age main sequence to post-main-sequence stage. The pulsation frequencies are calculated for every step in the evolutionary tracks. In the pulsation model calculation, f_0 and f_1 are considered to have the quantum numbers of $(l = 0, n = 1)$ and $(l = 0, n = 2)$, respectively.

Figure 5 shows the best-fit seismic models[5] to the observed frequencies along with the evolutionary tracks for

---

[5] More details can be found in Table 5.

Table 4. The observed stellar parameters of DY Peg.

Parameter	Value	Reference
[Fe/H] (dex)	-0.8 ± 0.2	Burki & Meylan (1986)
	-0.56	Peña et al. (1999)
	-0.8	Hintz et al. (2004)
T_{eff} (K)	[6750, 7950]	Burki & Meylan (1986)
	[6910, 8270]	Peña et al. (1999)
	[7330, 8230]	Hintz et al. (2004)
	[7200, 8350]	Kilambi & Rahman (1993)
$v \sin i$ (km s^{-1})	23.6	Solano & Fernley (1997)

specific combinations of (Z, v_{eq}), in which the subfigure (a) is a Petersen diagram (the period ratio of the first overtone mode to the fundamental mode (P_1/P_0) as a function of the fundamental mode period (P_0)) and the subfigure (b) is a Hertzsprung–Russell diagram (H-R diagram).[6] The nonradial modes are also calculated for these seismic models, and we find that f_2 with quantum numbers $(l = 1, n = 1)$ can give us the best-fit to the observed value.

In the H-R diagram, it is clear that the best-fit seismic models (based on single star evolution models) to the observed pulsation frequencies cannot match the observed temperature and luminosity. Furthermore, these seismic models cannot match a period change of $(1/P_0)(dP_0/dt) = -(5.87 \pm 0.03) \times 10^{-8}$ yr^{-1} either. Both of these discrepancies need additional interpretations.

4. DISCUSSION AND CONCLUSIONS

On one hand, the $O - C$ diagram provides us a clear evidence that the $O - C$ values could be well reproduced by a decrease of the pulsation period and a light traveling time effect of the star in a binary system of an elliptical orbit. On the other hand, the best-fit seismic models based on single star evolution show discrepancies with observed temperature and luminosity. All these results lead us to conclude that DY Peg should belong to a binary system.

In the subfigure (b) of Figure 5, we can consider that the dashed rectangle represents the temperature and luminosity of the binary system while the crosses repre-

---

[6] The range of the observed effective temperature $T_{\text{eff}} \in$ [6750, 8350] K is taken from related literatures (see the details in Table 4). The luminosity is calculated based on the distance, apparent magnitude, extinction, and bolometric correction. Considering the lightness variation of the star $\Delta V \sim 0.6$ mag, we finally get $\log L/L_\odot \in [1.07, 1.31]$. More details can be found in Section A of Appendix.

(a)

(b)
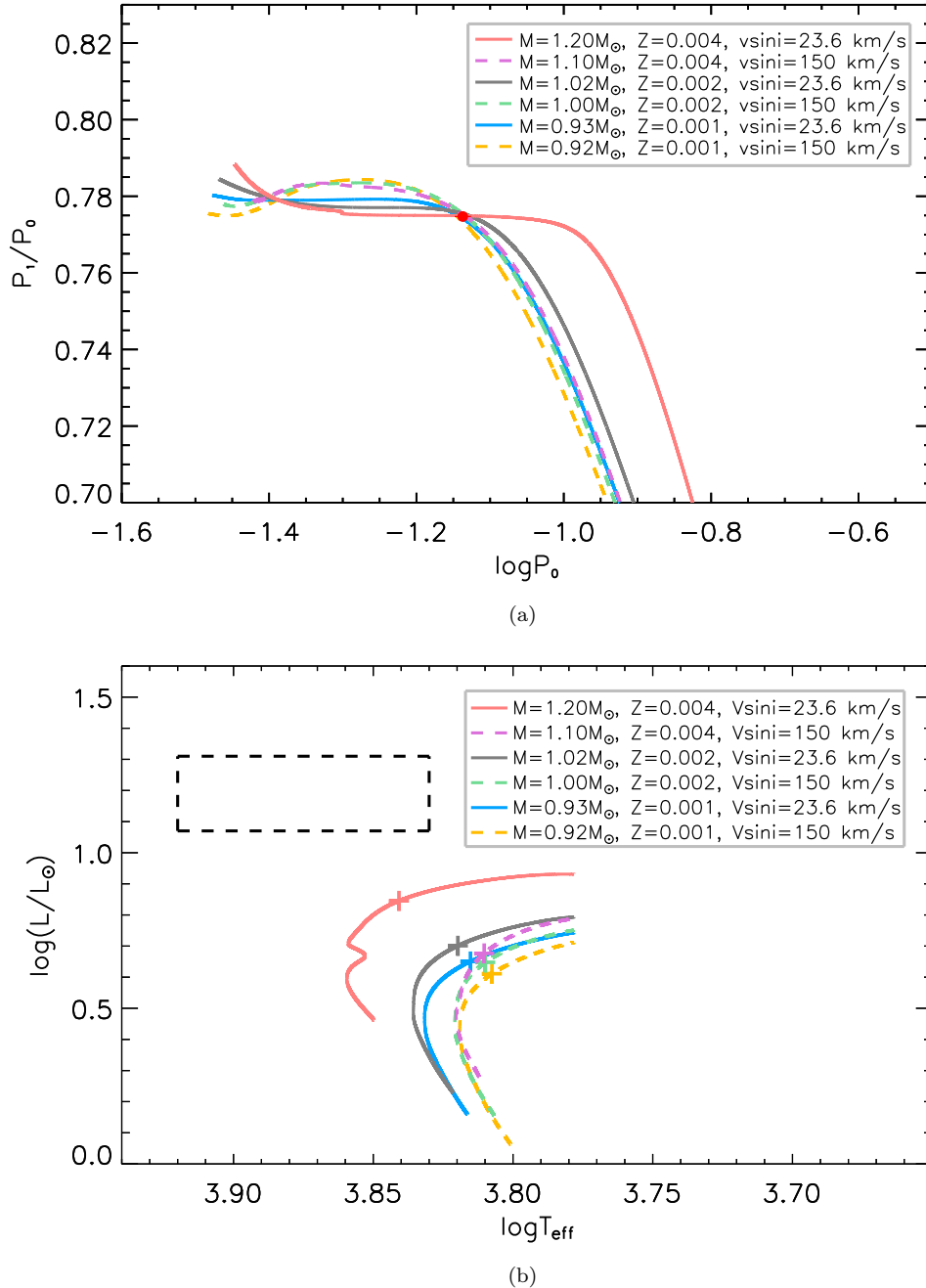
Figure 5. Six best seismic models for DY Peg along with the evolutionary tracks. In subfigure (a), the red point represents the observed value of P_1/P_0 and P_0 with uncertainties. In subfigure (b), the crosses on the evolutionary tracks represent the best seismic models; the region enclosed by dash lines is the domain of the observational values for the $\log(L/L_\odot)$ and $\log T_{\rm eff}$.

sent the possible models of DY Peg.[7] A hot companion and its added luminosity would make the combined photometric data for DY Peg, to appear hotter and more

---

[7] Here, we insist that there has not been a severe mass transfer process in the evolution history of DY Peg, whose orbital period can reach up to ~ 15400 days. Consequently, the best-fit seismic models based on single star evolution could also represent the properties of DY Peg.

luminous, as much is indicated by the dashed rectangle in the subfigure (b) of Fig. 5. Consequently, if the companion has higher temperature (hotter) and remarkable luminosity (not that faint), the discrepancy could hopefully be relieved. Additionally, according to the spectroscopic observations of DY Peg, Hintz et al. (2004) found a slight (0.15 dex) excess of the α-elements calcium and sulfur, and a more significant (0.5 dex) excess of carbon. Because these elements could only be produced

Table 5. Best-fit seismic models and the corresponding parameters.

Z	$v_{\rm eq}$ (km s^{-1})	M (M$_\odot$)	$T_{\rm eff}$ (K)	$\log L/L_\odot$	f_0 (c days^{-1})	f_1 (c days^{-1})	f_2 (c days^{-1})	f_0/f_1	$(1/P_0)(\mathrm{d}P_0/\mathrm{d}t)$ (yr^{-1})
0.001	23.6	0.93	6535	0.65	13.71241	17.7099	18.166	0.7743	1.1×10^{-9}
0.001	150	0.92	6421	0.61	13.71193	17.7305	18.373	0.7734	8.8×10^{-10}
0.002	23.6	1.02	6602	0.70	13.71301	17.6838	18.079	0.7754	9.7×10^{-10}
0.002	150	1.00	6455	0.65	13.71291	17.6864	18.222	0.7753	7.5×10^{-10}
0.004	23.6	1.20	6931	0.85	13.71327	17.6964	18.105	0.7749	9.7×10^{-10}
0.004	150	1.10	6461	0.68	13.71246	17.6869	18.130	0.7753	5.8×10^{-10}

in the phase of the asymptotic giant branch (AGB) via the s-process element enrichment or in the phase of the red giant (RG) via the helium burning, DY Peg's atmosphere should have been polluted by the companion that has already discarded its envelope and become a hot white dwarf (a sdB star cannot generate these elements in their evolutionary history (Han et al. 2002, 2003), nor can a brown dwarf).

Although we could not determine the mass of its companion because of the lack of information about the orbit inclination, we can reveal the relationship between the mass of the companion (M_2) and the orbit inclination (i) through the mass function obtained in Table 3. In Figure 6, it is obvious that the possibility of a brown dwarf companion is larger than that of a white dwarf companion, if we assume a random distribution of i (like that in Li & Qian (2010)). However, the above inference of a WD companion requires an orbit inclination $i \sim 5°$ if we consider the average mass of a WD ~ 0.6 $M_\odot$ (Tremblay et al. 2016).

Moreover, the decrease period change of the fundamental mode $(1/P_0)(\mathrm{d}P_0/\mathrm{d}t) = -(5.87 \pm 0.03) \times 10^{-8}$ yr^{-1} cannot be explained by the stellar evolution effect, which has been noted in previous works (see, e.g., Fu et al. (2009); Li & Qian (2010)) and has not been given a clear origin. In view of the above inferences, we interpret it as the result of the mass accretion from a dust disk around DY Peg, which was produced by the mass discarding of its companion in the AGB phase. This interpretation is obtained by the following considerations: (i) the mass accretion on DY Peg could result in a negative period change rate[8]; (ii) a direct mass transfer process from the companion to DY Peg is impossible, because the companion is not in its AGB phase and therefore cannot discard a large amount of matter now[9]; (iii) although a circumbinary disk is always re-

[8] This can be referred to in Eq. (7).

[9] Otherwise, it will show us a clear near-infrared excess from observations (Van Winckel 2018).

lated to post-AGB binary stars, the observed orbital periods of the systems range from 100 to about 3000 days, which are much smaller than the case of DY Peg (see Oomen et al. (2018) and references therein). Therefore, a dust disk around DY Peg should be a reasonable origin of its period change rate.

In such a case, the mass accretion rate of DY Peg can be calculated by the period-luminosity-color relation (Breger & Pamyatnykh 1998):

$$\log P = -0.3M_{bol} - 3\log T_{\rm eff} - 0.5\log M + \log Q + constant, \quad (6)$$

where P is the period of a radial mode of pulsation, M_{bol} is the bolometric absolute magnitude, $T_{\rm eff}$ is the effective temperature, M is the stellar mass in solar mass, and Q is the pulsation constant in days. We can get the expression of the period change rate by differentiating both side on time t:

$$\frac{1}{P}\frac{\mathrm{d}P}{\mathrm{d}t} = -0.69\frac{\mathrm{d}M_{bol}}{\mathrm{d}t} - \frac{3}{T_{\rm eff}}\frac{\mathrm{d}T_{\rm eff}}{\mathrm{d}t} - 0.5\frac{1}{M}\frac{\mathrm{d}M}{\mathrm{d}t} + \frac{1}{Q}\frac{\mathrm{d}Q}{\mathrm{d}t}. \quad (7)$$

If DY Peg follows a single star evolution without mass accretion, we have

$$\frac{1}{P}\frac{\mathrm{d}P}{\mathrm{d}t} = -0.69\frac{\mathrm{d}M_{bol}}{\mathrm{d}t} - \frac{3}{T_{\rm eff}}\frac{\mathrm{d}T_{\rm eff}}{\mathrm{d}t} + \frac{1}{Q}\frac{\mathrm{d}Q}{\mathrm{d}t}, \quad (8)$$

because $\mathrm{d}M/\mathrm{d}t = 0$.

In the case of mass accretion (which is denoted by $'$), we have

$$\frac{1}{P'}\frac{\mathrm{d}P'}{\mathrm{d}t} = -0.69\frac{\mathrm{d}M'_{bol}}{\mathrm{d}t} - \frac{3}{T'_{\rm eff}}\frac{\mathrm{d}T'_{\rm eff}}{\mathrm{d}t} - 0.5\frac{1}{M'}\frac{\mathrm{d}M'}{\mathrm{d}t} + \frac{1}{Q'}\frac{\mathrm{d}Q'}{\mathrm{d}t}. \quad (9)$$

In the above 2 equations, we assume $\mathrm{d}M_{bol}/\mathrm{d}t = \mathrm{d}M'_{bol}/\mathrm{d}t$, $(1/T_{\rm eff})(\mathrm{d}T_{\rm eff}/\mathrm{d}t) = (1/T'_{\rm eff})(\mathrm{d}T'_{\rm eff}/\mathrm{d}t)$, $(1/Q)(\mathrm{d}Q/\mathrm{d}t) = (1/Q')(\mathrm{d}Q'/\mathrm{d}t)$, $P = P'$, and $M = M'$. Then, the mass accretion rate ($\mathrm{d}M'/\mathrm{d}t$) can be calculated based on M, $P = 1/f_0$, and $(1/P)(\mathrm{d}P/\mathrm{d}t) = (1/P_0)(\mathrm{d}P_0/\mathrm{d}t)$ of the best-fit seismic models in Table 5, together with $(1/P')(\mathrm{d}P'/\mathrm{d}t) = -(5.87 \pm 0.03) \times 10^{-8}$ yr^{-1} in Table 3. Finally, the mass accretion rate

Figure 6. Relationship between the mass of the companion (M_2) and the orbit inclination (i). The red line and the blue dash line represent the relationships between M_2 and i when the mass of DY Peg (M_1) are equal to 0.92 $M_\odot$ and 1.20 $M_\odot$, respectively. The filled stars and squares are used to mark the lower limit mass of a white dwarf (0.15 $M_\odot$) and the upper limit mass of a brown dwarf (0.072 $M_\odot$) (Córsico 2020; Li & Qian 2010).

of DY Peg should be in the range of $[1.18 \times 10^{-7}, 1.19 \times 10^{-7}]$ $M_\odot$ yr^{-1}.

In summary, in this work, we have (i) detected and confirmed $f_2 = 18.138$ c days^{-1} as a nonradial pulsation mode with quantum numbers ($l = 1$, $n = 1$) for the first time; (ii) confirmed DY Peg belongs to a binary system with an orbital period $P_{orb} = 15425.0 \pm 205.7$ days; (iii) confirmed the period change rate of fundamental mode of DY Peg $(1/P_0)(\,dP_0/\,dt) = -(5.87 \pm 0.03) \times 10^{-8}$ yr^{-1}; and (iv) combined the information from observation and theoretical calculation and inferred that DY Peg should be accreting mass from a dust disk, which was the residue of its evolved companion (most probably a hot WD at the present stage) in the AGB phase. In order to confirm the inferences, more precise spectroscopic and photometric observations are needed. Whether every SX Phe star has an evolutionary history in a binary system, whose companion is an evolved star after the AGB phase and has produced a dust disk around it, should be tested and verified in the future.

REFERENCES

Arellano Ferro, A., Ahumada, J. A., Kains, N., & Luna, A. 2016, MNRAS, 461, 1032, doi: 10.1093/mnras/stw1358

Asplund, M., Grevesse, N., Sauval, A. J., & Scott, P. 2009, ARA&A, 47, 481, doi: 10.1146/annurev.astro.46.060407.145222

Bailer-Jones, C. A. L., Rybizki, J., Fouesneau, M., Mantelet, G., & Andrae, R. 2018, AJ, 156, 58, doi: 10.3847/1538-3881/aacb21

Barcza, S., & Benkő, J. M. 2014, MNRAS, 442, 1863, doi: 10.1093/mnras/stu978

Breger, M., & Pamyatnykh, A. A. 1998, A&A, 332, 958

Burki, G., & Meylan, G. 1986, A&A, 159, 261

Córsico, A. H. 2020, Frontiers in Astronomy and Space Sciences, 7, 47, doi: 10.3389/fspas.2020.00047

Derekas, A., Kiss, L. L., Székely, P., et al. 2003, A&A, 402, 733, doi: 10.1051/0004-6361:20030291

Derekas, A., Kiss, L. L., Bedding, T. R., et al. 2009, MNRAS, 394, 995, doi: 10.1111/j.1365-2966.2008.14381.x

Foreman-Mackey, D., Hogg, D. W., Lang, D., & Goodman, J. 2013, PASP, 125, 306, doi: 10.1086/670067

Fu, J.-N., Zhang, C., Marak, K., et al. 2008, ChJA&A, 8, 237, doi: 10.1088/1009-9271/8/2/11

Fu, J. N., Zha, Q., Zhang, Y. P., et al. 2009, PASP, 121, 251, doi: 10.1086/597829

Garrido, R., & Rodriguez, E. 1996, MNRAS, 281, 696, doi: 10.1093/mnras/281.2.696

Goldstein, H., Poole, C., & Safko, J. 2002, Classical mechanics

Han, Z., Podsiadlowski, P., Maxted, P. F. L., & Marsh, T. R. 2003, MNRAS, 341, 669, doi: 10.1046/j.1365-8711.2003.06451.x

Han, Z., Podsiadlowski, P., Maxted, P. F. L., Marsh, T. R., & Ivanova, N. 2002, MNRAS, 336, 449, doi: 10.1046/j.1365-8711.2002.05752.x

Henden, A. A., Templeton, M., Terrell, D., et al. 2016, VizieR Online Data Catalog, II/336

Hintz, E. G., Joner, M. D., Ivanushkina, M., & Pilachowski, C. A. 2004, PASP, 116, 543, doi: 10.1086/420858

Hübscher, J. 2011, Information Bulletin on Variable Stars, 5984, 1

—. 2014, Information Bulletin on Variable Stars, 6118, 1

—. 2015, Information Bulletin on Variable Stars, 6152, 1

—. 2017, BAV Journal, 013, 1

Hübscher, J., Braune, W., & Lehmann, P. B. 2013, Information Bulletin on Variable Stars, 6048, 1

Hübscher, J., & Lehmann, P. B. 2012, Information Bulletin on Variable Stars, 6026, 1

—. 2013, Information Bulletin on Variable Stars, 6070, 1

Hübscher, J., Lehmann, P. B., Monninger, G., Steinbach, H.-M., & Walter, F. 2010, Information Bulletin on Variable Stars, 5941, 1

Iriarte, B. 1952, ApJ, 116, 382, doi: 10.1086/145621

Irwin, J. B. 1952, ApJ, 116, 211, doi: 10.1086/145604

Jones, D., & Boffin, H. M. J. 2017, Nature Astronomy, 1, 0117, doi: 10.1038/s41550-017-0117

Kafka, S. 2020, Observations from the AAVSO International Database. https://www.aavso.org

Kilambi, G. C., & Rahman, A. 1993, Bulletin of the Astronomical Society of India, 21, 573

Landau, L. D., & Lifshitz, E. M. 1969, Mechanics

Lenz, P., & Breger, M. 2005, Communications in Asteroseismology, 146, 53, doi: 10.1553/cia146s53

Li, L. J., & Qian, S. B. 2010, AJ, 139, 2639, doi: 10.1088/0004-6256/139/6/2639

Mahdy, H. A., & Szeidl, B. 1980, Commmunications of the Konkoly Observatory Hungary, 74, 1

McNamara, D. H. 2011, AJ, 142, 110, doi: 10.1088/0004-6256/142/4/110

Meylan, G., Burki, G., Rufener, F., et al. 1986, A&AS, 64, 25

Montgomery, M. H., & Odonoghue, D. 1999, Delta Scuti Star Newsletter, 13, 28

Morgenroth, O. 1934, Astronomische Nachrichten, 252, 389, doi: 10.1002/asna.19342522402

Mowlavi, N., Meynet, G., Maeder, A., Schaerer, D., & Charbonnel, C. 1998, A&A, 335, 573

Niu, J.-S., & Li, T. 2018, PhRvD, 97, 023015, doi: 10.1103/PhysRevD.97.023015

Niu, J.-S., Li, T., Ding, R., et al. 2018, PhRvD, 97, 083012, doi: 10.1103/PhysRevD.97.083012

Niu, J.-S., Li, T., & Xue, H.-F. 2019, ApJ, 873, 77, doi: 10.3847/1538-4357/ab0420

Niu, J.-S., Fu, J.-N., Li, Y., et al. 2017, MNRAS, 467, 3122, doi: 10.1093/mnras/stx125

Oomen, G.-M., Van Winckel, H., Pols, O., et al. 2018, A&A, 620, A85, doi: 10.1051/0004-6361/201833816

Paparo, M., Szeidl, B., & Mahdy, H. A. 1988, Ap&SS, 149, 73, doi: 10.1007/BF00640467

Paxton, B., Bildsten, L., Dotter, A., et al. 2011, ApJS, 192, 3, doi: 10.1088/0067-0049/192/1/3

Paxton, B., Cantiello, M., Arras, P., et al. 2013, ApJS, 208, 4, doi: 10.1088/0067-0049/208/1/4

Paxton, B., Marchant, P., Schwab, J., et al. 2015, ApJS, 220, 15, doi: 10.1088/0067-0049/220/1/15

Paxton, B., Schwab, J., Bauer, E. B., et al. 2018, ApJS, 234, 34, doi: 10.3847/1538-4365/aaa5a8

Paxton, B., Smolec, R., Schwab, J., et al. 2019, ApJS, 243, 10, doi: 10.3847/1538-4365/ab2241

Peña, J. H., González, D., & Peniche, R. 1999, A&AS, 138, 11, doi: 10.1051/aas:1999264

Pena, J. H., & Peniche, R. 1986, A&A, 166, 211

Percy, J. R., Bandara, K., & Cimino, P. 2007, Journal of the American Association of Variable Star Observers (JAAVSO), 35, 343

Petersen, J. O., & Christensen-Dalsgaard, J. 1996, A&A, 312, 463

—. 1999, A&A, 352, 547

Pop, A., Turcu, V., & Moldovan, D. 2003, in Astronomical Society of the Pacific Conference Series, Vol. 292, Interplay of Periodic, Cyclic and Stochastic Variability in Selected Areas of the H-R Diagram, ed. C. Sterken, 141

Poretti, E., Suárez, J. C., Niarchos, P. G., et al. 2005, A&A, 440, 1097, doi: 10.1051/0004-6361:20053463

Quigley, R., & Africano, J. 1979, PASP, 91, 230, doi: 10.1086/130476

Rodríguez, E., & Breger, M. 2001, A&A, 366, 178, doi: 10.1051/0004-6361:20000205

Rodríguez, E., & López-González, M. J. 2000, A&A, 359, 597

Schlafly, E. F., & Finkbeiner, D. P. 2011, The Astrophysical Journal, 737, 103, doi: 10.1088/0004-637x/737/2/103

Solano, E., & Fernley, J. 1997, A&AS, 122, 131, doi: 10.1051/aas:1997329

Torres, G. 2010, The Astronomical Journal, 140, 1158, doi: 10.1088/0004-6256/140/5/1158

Townsend, R. H. D., & Teitler, S. A. 2013, MNRAS, 435, 3406, doi: 10.1093/mnras/stt1533

Tremblay, P. E., Cummings, J., Kalirai, J. S., et al. 2016, MNRAS, 461, 2100, doi: 10.1093/mnras/stw1447

Van Winckel, H. 2018, arXiv e-prints, arXiv:1809.00871. https://arxiv.org/abs/1809.00871

Wils, P., Hambsch, F.-J., Lampens, P., et al. 2010, Information Bulletin on Variable Stars, 5928, 1

Wils, P., Hambsch, F.-J., Robertson, C. W., et al. 2011, Information Bulletin on Variable Stars, 5977, 1

Wils, P., Panagiotopoulos, K., van Wassenhove, J., et al. 2012, Information Bulletin on Variable Stars, 6015, 1

Wils, P., Ayiomamitis, A., Vanleenhove, M., et al. 2013, Information Bulletin on Variable Stars, 6049, 1

Wils, P., Hambsch, F.-J., Vanleenhove, M., et al. 2015, Information Bulletin on Variable Stars, 6150, 1

Xue, H.-F., Fu, J.-N., Fox-Machado, L., et al. 2018, ApJ, 861, 96, doi: 10.3847/1538-4357/aac9c5

Yang, X. H., Fu, J. N., & Zha, Q. 2012, AJ, 144, 92, doi: 10.1088/0004-6256/144/4/92

APPENDIX

A. ESTIMATION OF THE LUMINOSITY

The visual absolute magnitude M_V can be expressed as

$$M_V = V - 5 \log d + 5 - A_V, \tag{A1}$$

where $V = 10.264$ mag is taken from AAVSO Photometric All Sky Survey (APASS) catalog (Henden et al. 2016). The distance $d = 404$ pc is provided by Gaia DR2 (Bailer-Jones et al. 2018). The extinction $A_V = 0.363$ mag is obtained from the maps of Schlafly & Finkbeiner (2011).

The absolute bolometric magnitude $M_{\rm bol}$ can be calculated from

$$M_{\rm bol} = M_V + BC, \tag{A2}$$

where the empirical bolometric correction

$$BC = 0.128 \log P + 0.022 \tag{A3}$$

for δ Scuti stars is derived by Petersen & Christensen-Dalsgaard (1999).

Then the luminosity can be obtained via $\log L/L_\odot = -0.4(M_{\rm bol} - M_{\rm bol,\odot})$. Here, the bolometric magnitude of the Sun $M_{\rm bol,\odot}$ is taken to be 4.73 mag (Torres 2010). The range of the luminosity is estimated based on the lightness variation of the star, $\Delta V \sim 0.6$ mag. Finally, we get the range of the observed luminosity as $\log L/L_\odot \in [1.07, 1.31]$.

B. MATHEMATICAL DEDUCTION OF THE EQUATIONS

In this section, we show a brief deduction of Eq. (1) and (2). The geometric elements in the elliptic orbit of a celestial body (M) in a binary system are shown in Figure B1, and the position of the elliptic orbit in the sky is shown in Figure B2.

In the first subsection, we will construct the relationship between the light-time perturbation and the angle variables which represent the position of M in the elliptic orbit. In the second section, we will construct the relationship between the time interval starting from a reference point (when one of the celestial body passages through the periastron) and the angle variables that represent the position of M in the elliptic orbit.

B.1. *Aspect of Geometry*

Because a clear deduction of the pulsation part in Eq. (1) has been represented in Arellano Ferro et al. (2016), we focus on the last term (the binary part) in Eq. (1).

In Figure B1, we define $r \equiv$ FM, which is the distance from the focus F to the position of the celestial body M. Then, r can be represented in the polar coordinate system as

$$r = \frac{p}{1 + e \cos \nu} = \frac{a(1 - e^2)}{1 + e \cos \nu}, \tag{B4}$$

where p is the semi-focal chord, e is the eccentricity (here $0 < e < 1$), ν is the true anomaly, and a is the length of the semi-major axis. It is not difficult to obtain the relationship between ν and ϕ in Figure B1:

$$\sin \phi = \sqrt{1 - e^2} \frac{\sin \nu}{1 + e \cos \nu}, \quad \cos \phi = \frac{e + \cos \nu}{1 + e \cos \nu}, \quad \tan \frac{\phi}{2} = \sqrt{\frac{1 - e}{1 + e}} \tan \frac{\nu}{2}. \tag{B5}$$

In Figure B2, we define $\omega \equiv \angle$AFE (which denotes the angle from the ascending node to periastron in the orbital plane) and $i \equiv \angle$SCT (which denotes the orbit inclination). The existence of a companion causes a light-time perturbation when the variable star goes along its elliptic orbit, which crosses the plane α. As a result, the last term (the binary part) in Eq. (1) accounts for the time which light travels from the position of the celestial body (M) to α in the direction of $\overrightarrow{\rm CS}$. The distance from the position of the celestial body (M) to β in the direction of $\overrightarrow{\rm CS}$ can be expressed as

$$z = r \sin i \sin (\nu + \omega), \tag{B6}$$
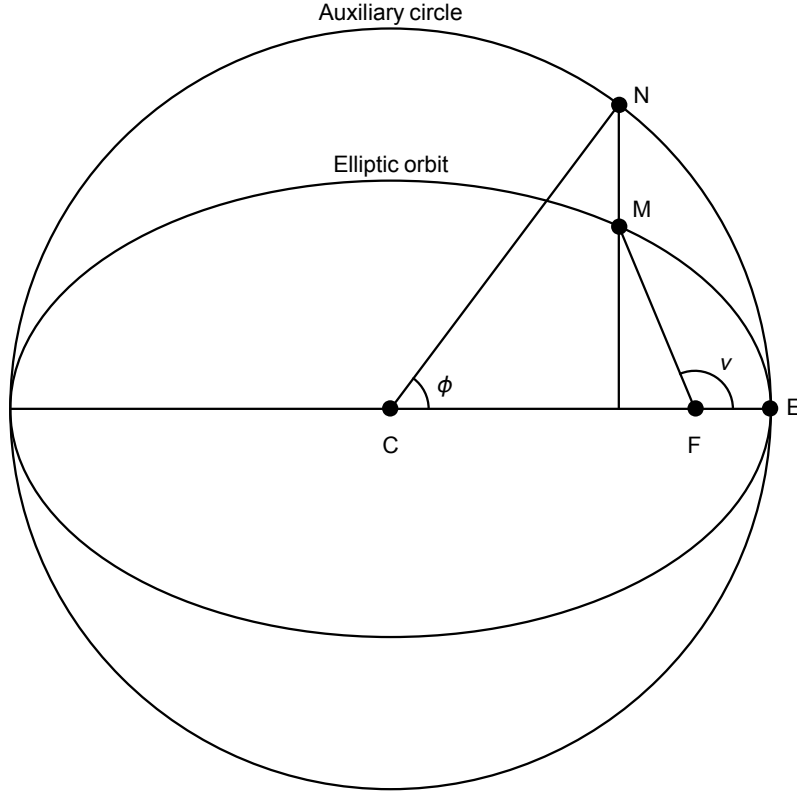
Figure B1. Geometric elements in the elliptic orbit of a celestial body in a binary system. The elliptic orbit shows the orbit of M (which denotes the position of the celestial body), C denotes the center of the elliptic orbit, F denotes the mass center of the binary system (which is also one of the focuses of the elliptic orbit), E denotes the periastron, and $\nu \equiv \angle$EFM denotes the true anomaly. The auxiliary circle has the center C and radius equal to the length of the semi-major axis of the elliptic orbit. N is the point of intersection between the line through M (which is perpendicular to CF) and the auxiliary circle. $\phi \equiv \angle$ECN denotes the eccentric anomaly.

and the distance from M to α can be expressed as

$$z' = z + ae \sin \omega \sin i = r \sin i \sin (\nu + \omega) + ae \sin \omega \sin i. \tag{B7}$$

Now, it is obvious that the light-time perturbation (τ) has the form

$$\tau = \frac{z'}{c} = \frac{r \sin i \sin (\nu + \omega) + ae \sin \omega \sin i}{c} \tag{B8}$$

$$= \frac{a \sin i}{c} \left[(1 - e^2) \frac{\sin (\nu + \omega)}{1 + e \cos \nu} + e \sin \omega \right] \quad \text{(Eq. B4)} \tag{B9}$$

$$= \frac{a \sin i}{c} \left[\sqrt{1 - e^2} \sin \phi \cos \omega + \cos \phi \sin \omega \right] \quad \text{(Eq. B5)} \tag{B10}$$

$$= A \left[\sqrt{1 - e^2} \sin \phi \cos \omega + \cos \phi \sin \omega \right] \quad (A \equiv \frac{a \sin i}{c}), \tag{B11}$$

where c is the speed of light in vacuum.

B.2. *Aspect of Dynamics*

Let us consider two mass points (M and m) gravitationally revolving around each other in an elliptic orbit. m_1 and m_2 are the mass of M and m, $\mathbf{r_1}$ and $\mathbf{r_2}$ are the radii vectors of M and m relative to the center of mass. If we define $\mathbf{r} = \mathbf{r_1} - \mathbf{r_2} = r\hat{\mathbf{r}}$ (where r is the length of $\mathbf{r}$, and $\hat{\mathbf{r}}$ is the unit vector parallel to $\mathbf{r}$), we have

$$\mathbf{r_1} = \frac{m_2}{m_1 + m_2}\mathbf{r}, \tag{B12}$$
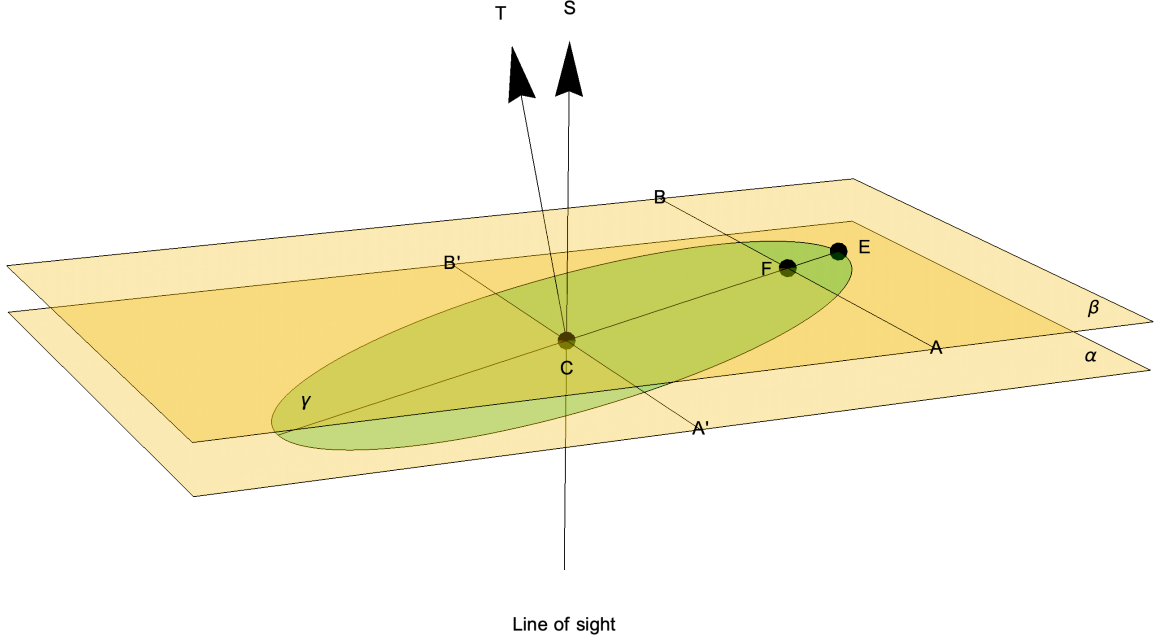
Figure B2. Position of the elliptic orbit in the sky. γ denotes the orbit plane of the celestial body M in the binary system. The meanings of C, F, and E are the same as those in Figure B1. $\overrightarrow{CT}$ denotes the direction perpendicular to γ, and $\overrightarrow{CS}$ denotes the direction of the line of sight. α denotes the plane through the center of the elliptic orbit that is perpendicular to $\overrightarrow{CS}$ and has a line of intersection A'B' with γ. β denotes the plane through the mass center (one of the focuses) of the elliptic orbit that is perpendicular to $\overrightarrow{CS}$ and has a line of intersection AB with γ.

$$\mathbf{r_2} = -\frac{m_1}{m_1 + m_2}\mathbf{r}. \tag{B13}$$

In the polar coordinate system, following Kepler's second law, we have

$$\frac{1}{2}r^2\dot{\nu} = \frac{1}{2}h, \tag{B14}$$

where h is a constant.

Solving the above two body problem gravitationally, one can get the orbital equation (see, e.g., Landau & Lifshitz (1969); Goldstein et al. (2002))

$$r = \frac{p}{1 + e\cos\nu} = \frac{h^2/\mu}{1 + e\cos\nu} = \frac{b^2/a}{1 + e\cos\nu}, \tag{B15}$$

and the orbital period of the binary system

$$P_{\mathrm{orb}} = 2\pi\sqrt{\frac{a^3}{\mu}} = \frac{2\pi ab}{h}, \tag{B16}$$

where $p = h^2/\mu = b^2/a$ is the semi-focal chord, $\mu = G(m_1 + m_2)$, a is the length of semi-major axis, b is length of the semi-minor axis, and G is the gravitational constant.

Substituting Eq. (B15) into Eq. (B14), we get

$$\frac{1}{(1 + e\cos\nu)^2}\, d\nu = \frac{\mu^2}{h^3}\, dt. \tag{B17}$$

Integrating the above equation, we have

$$\int_0^\nu \frac{1}{(1 + e\cos\theta)^2}\, d\theta = \frac{\mu^2}{h^3}(t - t_0), \tag{B18}$$

where t_0 is reference time when $\nu = 0$. It is the time when M (and m) passages through the periastron in our case.

Because $0 < e < 1$ in Eq. (B18), the integral in it can be integrated and Eq. (B18) can be translated as follows:

$$\frac{1}{(1 - e^2)^{3/2}}\left[2\arctan\left(\sqrt{\frac{1 - e}{1 + e}}\tan\frac{\nu}{2}\right) - \frac{e\sqrt{1 - e^2}\sin\nu}{e\cos\nu + 1}\right] = \frac{\mu^2}{h^3}(t - t_0). \tag{B19}$$

Let us employ the mean anomaly Φ as follows

$$\Phi = \frac{2\pi}{P_{\rm orb}}(t - t_0) = \sqrt{\frac{\mu}{a^3}}(t - t_0) = \frac{\mu^2}{h^3}(1 - e^2)^{3/2}(t - t_0). \tag{B20}$$

Replacing ν (true anomaly) with ϕ (eccentric anomaly) (Eq. (B5)) and t with Φ (Eq. (B20)) in Eq. (B19), we get

$$\phi - e\sin\phi = \Phi. \tag{B21}$$

Noting the relationships in Eq. (B12) and (B13), the elliptic orbits of M and m can be expressed as

$$r_1 = \frac{m_2}{m_1 + m_2}\frac{p}{1 + e\cos\nu} = \frac{m_2}{m_1 + m_2}\frac{h^2/\mu}{1 + e\cos\nu} = \frac{m_2}{m_1 + m_2}\frac{b^2/a}{1 + e\cos\nu}, \tag{B22}$$

and

$$r_2 = \frac{m_1}{m_1 + m_2}\frac{p}{1 + e\cos\nu} = \frac{m_1}{m_1 + m_2}\frac{h^2/\mu}{1 + e\cos\nu} = \frac{m_1}{m_1 + m_2}\frac{b^2/a}{1 + e\cos\nu}, \tag{B23}$$

which imply $\nu = \nu_1 = -\nu_2$, $e = e_1 = e_2$, and $P_{\rm orb} = P_{{\rm orb},1} = P_{{\rm orb},2}$. Consequently, we have $\Phi = \Phi_1 = \Phi_2$ and $\phi = \phi_1 = -\phi_2$.

At last, we get

$$\phi_1 - e_1\sin\phi_1 = \Phi_1 \tag{B24}$$

for M, and

$$-\phi_2 + e_2\sin\phi_2 = \Phi_2 \tag{B25}$$

for m.

C. LONG TABLES

Table C1. Newly determined times of maximum light for DY Peg.

HJD (2400000+)	σ	HJD (2400000+)	σ	HJD (2400000+)	σ	HJD (2400000+)	σ
52877.72438	0.00004	54406.32897	0.00005	55883.59358	0.00001	57671.66867	0.00002
52877.79792	0.00004	54411.50742	0.00002	55883.66642	0.00001	57671.73953	0.00002
52882.68303	0.00004	54411.57987	0.00002	55883.73958	0.00001	57988.38614	0.00004
52882.75695	0.00004	54467.58710	0.00004	55893.58410	0.00001	58005.59641	0.00002
52884.72583	0.00003	54485.59983	0.00007	55893.65691	0.00001	58005.66960	0.00003
52885.74570	0.00005	54701.82562	0.00004	55894.53214	0.00001	58005.74262	0.00002
52886.69385	0.00003	54702.84695	0.00003	55894.60485	0.00001	58005.81525	0.00002
52886.76697	0.00003	54720.71394	0.00004	55894.67813	0.00002	58005.88827	0.00005
52896.68489	0.00004	54720.78651	0.00004	55896.57398	0.00001	58055.33167	0.00007
52896.75809	0.00004	55122.68311	0.00007	55896.64710	0.00001	58055.40499	0.00007
52902.66618	0.00005	55122.75635	0.00007	56133.43755	0.00003	58071.37567	0.00002
52902.73851	0.00006	55418.51286∗	0.00006	56165.3805	0.0001	58071.52164	0.00003
53252.78456	0.00004	55445.38032	0.00002	56223.35532	0.00002	58308.53186	0.00008
53295.21598∗	0.00009	55445.45321	0.00002	56223.42830	0.00004	58348.4219	0.0001
53973.73189	0.00003	55445.52690	0.00003	56223.50190	0.00009	58348.49447	0.00007
53975.70061	0.00007	55478.48918	0.00007	56987.69433	0.00002	58362.42380	0.00006
53983.3584	0.0002	55806.51075	0.00001	57002.35206	0.00009	58362.49652	0.00006
53997.65161	0.00006	55834.36863	0.00001	57296.31755	0.00001	58363.44508	0.00006
54003.70445	0.00002	55848.44268	0.00004	57296.38996	0.00002	58369.78916	0.00006
54012.74724	0.00001	55848.51586	0.00005	57296.46383	0.00002	58416.53503	0.00009
54020.69599	0.00002	55864.55996	0.00001	57299.23559	0.00004	58657.55576	0.00004
54020.76879	0.00002	55864.70577	0.00001	57300.40170	0.00005	58657.62869	0.00004
54266.82149	0.00002	55864.77902	0.00003	57300.47481	0.00006	58681.47490	0.00012
54325.74580	0.00006	55866.60212	0.00001	57305.57883	0.00003	58703.42637	0.00007
54325.81846	0.00007	55866.67516	0.00001	57305.65153	0.00004	58703.49882	0.00008
54325.89178	0.00006	55866.74708	0.00004	57312.57982	0.00003	58725.59537	0.00004
54332.67356	0.00006	55867.54975	0.00001	57312.65253	0.00004	58725.66842	0.00002
54332.74681	0.00007	55867.62276	0.00001	57327.31131	0.00004	58725.74119	0.00004
54332.81953	0.00006	55867.69561	0.00001	57646.58186	0.00003	58725.81485	0.00002
54332.89248	0.00008	55867.76839	0.00003	57646.65474	0.00002	58725.88742	0.00003
54386.56584	0.00003	55869.59154	0.00001	57646.72669	0.00002	58748.34909	0.00001
54398.67219	0.00008	55869.66473	0.00001	57646.80075	0.00002	58760.67399	0.00002
54398.74495	0.00007	55876.59286	0.00001	57646.87287	0.00003	58760.74599	0.00002
54398.81767	0.00006	55876.66585	0.00001	57671.52163	0.00003	58781.52988	0.00003
54406.25626	0.00005	55876.73841	0.00002	57671.59525	0.00002		

NOTE—asterisks represent the data are not used in $O - C$ analysis.

Table C2. Times of maximum light for DY Peg published in Hübscher et al. (2010, 2013); Hübscher (2011, 2014, 2015, 2017); Hübscher & Lehmann (2012, 2013); Wils et al. (2010, 2011, 2012, 2013, 2015).

HJD (2400000+)	σ	Ref.	HJD (2400000+)	σ	Ref.	HJD (2400000+)	σ	Ref.
54736.3201	0.0004	(1)	55464.7784	0.0002	(4)	55858.4334	0.0006	(6)
54736.3926	0.0005	(1)	55464.8514	0.0003	(4)	55859.3820	0.0009	(6)
54736.4660	0.0005	(1)	55464.9245	0.0005	(4)	55867.3309	0.0006	(6)
54737.2680	0.0006	(1)	55466.6018	0.0002	(4)	55867.4040	0.0006	(6)
54737.3409	0.0005	(1)	55466.6747	0.0002	(4)	55877.3217	0.0008	(6)
54737.4136	0.0004	(1)	55466.7476	0.0006	(4)	55878.3419	0.0006	(6)
55069.3734	0.0004	(2)	55466.8201	0.0004	(4)	55879.3634	0.0014	(6)
55069.4458	0.0003	(2)	55466.8937	0.0004	(4)	55879.4366	0.0019	(6)
55069.5190	0.0002	(2)	55468.6439	0.0003	(4)	55879.5106	0.0009	(6)
55069.5923	0.0002	(2)	55468.7165	0.0003	(4)	55886.2915	0.0006	(6)
55074.4778	0.0006	(1)	55468.7893	0.0002	(4)	55893.2923	0.0008	(6)
55074.5511	0.0004	(1)	55468.8627	0.0002	(4)	55893.3654	0.0014	(6)
55074.6241	0.0006	(1)	55468.9354	0.0007	(4)	55893.4377	0.0008	(6)
55093.3656	0.0035	(3)	55470.6126	0.0002	(4)	55894.3133	0.0007	(6)
55113.4203	0.0009	(2)	55470.6856	0.0002	(4)	55894.3872	0.0009	(6)
55113.4933	0.0006	(2)	55470.7583	0.0004	(4)	55896.2829	0.0001	(6)
55130.2666	0.0003	(2)	55470.8312	0.0003	(4)	55896.3552	0.0008	(6)
55132.3811	0.0006	(2)	55478.3428	0.0005	(1)	55903.2832	0.0012	(7)
55143.3929	0.0007	(2)	55478.4163	0.0005	(1)	55903.3564	0.0004	(7)
55155.2806	0.0005	(1)	55796.5192	0.0028	(6)	55903.4292	0.0002	(7)
55155.3534	0.0004	(2)	55806.3643	0.0004	(7)	55908.2422	0.0009	(6)
55155.4266	0.0001	(2)	55806.4374	0.0005	(7)	55908.3145	0.0003	(6)
55177.3767	0.0007	(2)	55814.3864	0.0004	(1)	56133.4374	0.0008	(8)
55180.2940	0.0008	(2)	55814.4597	0.0004	(1)	56175.5164	0.0003	(8)
55180.3671	0.0006	(2)	55814.5323	0.0004	(1)	56175.5891	0.0007	(8)
55192.2535	0.0002	(2)	55833.4192	0.0021	(6)	56180.4024	0.0005	(9)
55192.3270	0.0006	(2)	55835.4623	0.0004	(6)	56180.4751	0.0004	(9)
55371.5791	0.0008	(1)	55836.4099	0.0006	(6)	56190.3965	0.0035	(10)
55371.5791	0.0005	(1)	55836.4831	0.0006	(6)	56200.3840	0.0035	(11)
55409.7914	0.0007	(4)	55837.4307	0.0005	(6)	56223.3549	0.0007	(8)
55409.8670	0.0013	(4)	55837.5046	0.0008	(6)	56223.4277	0.0006	(8)
55439.4733	0.0035	(5)	55848.3705	0.0009	(6)	56223.5011	0.0006	(8)
55444.5053	0.0014	(5)	55848.4420	0.0005	(6)	56495.4445	0.0069	(10)
55445.3798	0.0007	(4)	55848.4427	0.0004	(7)	56514.4034	0.0035	(10)
55445.4527	0.0003	(4)	55848.5157	0.0002	(7)	56622.3342	0.0035	(10)
55445.5260	0.0003	(4)	55849.3909	0.0007	(6)	56900.4755	0.0011	(12)
55446.4011	0.0028	(5)	55849.4641	0.0007	(6)	56900.5479	0.0004	(12)

Table C2 *continued*

Table C2 *(continued)*

HJD (2400000+)	σ	Ref.	HJD (2400000+)	σ	Ref.	HJD (2400000+)	σ	Ref.
55451.5064	0.0028	(5)	55849.5366	0.0008	(6)	56900.6210	0.0003	(12)
55453.3285	0.0035	(5)	55852.4536	0.0004	(1)	56981.3496	0.0035	(11)
55459.6009	0.001	(4)	55854.2768	0.0003	(7)	56981.4225	0.0035	(11)
55459.6738	0.0004	(4)	55854.3501	0.0002	(7)	57002.3529	0.0004	(12)
55459.7464	0.0002	(4)	55856.3923	0.0004	(6)	57296.3070∗	0.0004	(13)
55459.8196	0.0003	(4)	55856.4648	0.0005	(6)	57296.3799∗	0.0004	(13)
55459.8924	0.0006	(4)	55857.3400	0.0006	(6)	57296.4531∗	0.0005	(13)
55464.6327	0.0002	(4)	55857.4130	0.001	(6)	57296.5260∗	0.0004	(13)
55464.7053	0.0003	(4)	55857.4853	0.0007	(6)	57296.5984∗	0.0005	(13)

NOTE—asterisks represent the data are not used in $O - C$ analysis.

References—(1) Hübscher et al. (2013); (2) Wils et al. (2010); (3) Hübscher et al. (2010); (4) Wils et al. (2011); (5) Hübscher (2011); (6) Hübscher & Lehmann (2012); (7) Wils et al. (2012); (8) Wils et al. (2013); (9) Hübscher & Lehmann (2013); (10) Hübscher (2014); (11) Hübscher (2015); (12) Wils et al. (2015); (13) Hübscher (2017).